Biochimica et Biophysica Acta 1838 (2014) 766–775

Contents lists available at ScienceDirect

Biochimica et Biophysica Acta

journal homepage: www.elsevier.com/locate/bbamem

Electrophoretic mobility of sarcoplasmic reticulum vesicles — Analytical model includes amino acid residues of A + P + N domain of Ca^{2+}-ATPase and charged lipids

Pavel Smejtek *, Robert C. Word, Laura E. Satterfield

Department of Physics and Molecular Biosciences Group, Portland State University, Portland, OR 97207-0751, USA

ARTICLE INFO

Article history:
Received 28 June 2013
Received in revised form 23 September 2013
Accepted 25 September 2013
Available online 4 October 2013

Keywords:
Electrophoretic mobility
pH dependence
Sarcoplasmic reticulum vesicle
Ca^{2+}-ATPase
Calcium pump layer

ABSTRACT

This work is an experimental and theoretical study of electrostatic and hydrodynamic properties of the surface of sarcoplasmic reticulum (SR) membrane using particle electrophoresis. The essential structural components of SR membrane include a lipid matrix and a dense layer of Ca^{2+}-ATPases embedded in the matrix. The Ca^{2+}-ATPase layer both drives and impedes vesicle mobility. To analyze the experimental mobility data, obtained at pH 4.0, 4.7, 5.0, 6.0, 7.5, and 9.0 in 0.1 M monovalent (1:1) electrolyte, an analytical solution for the vesicle mobility and electroosmotic flow velocity distribution was obtained by solving the Poisson–Boltzmann and the Navier–Stokes–Brinkman equations. The electrophoretic mobility model includes two sets of charges that represent: (a) charged lipids of the lipid matrix of the vesicle core, and (b) charged amino acid residues of APN domains of Ca^{2+}-ATPases. APN domains are assumed to form a charged plane displaced from the surface of lipid matrix. The charged plane is embedded in a frictional layer that represents the surface layer of calcium pumps. Electrophoretic mobility is driven by the charged APN domain and by lipid matrix while the surface layer provides hydrodynamic friction. The charge of APN domain is determined by ionized amino acid residues obtained from the amino acid composition of SERCA1a Ca^{2+}-ATPase. Agreement between the measured and the predicted mobility is evaluated by the weighted sum of mobility deviation squared. This model reproduces the experimental dependence of mobility on pH and predicts that APN domains are located in the upper half of the SR vesicle surface layer.

1. Introduction and background

Liposomes and vesicles prepared from biological membranes play a critical role in studies of their structure and function, as well as the development of special applications of biological and synthetic membranes. Sarcoplasmic reticulum (SR) vesicles are spherical particles made out of sarcoplasmic reticulum membrane as an envelope. The interior of the vesicles is filled with aqueous salt solution suspending the vesicles.

Electrophoretic mobility studies in which the molecular composition of membrane, the pH, and the salt concentration are experimental variables play a prominent role in developing insight into structure–function relationships. Initially these studies were based on Helmholtz–Smoluchowski concepts that were later expanded into the "standard electrokinetic model" [1]. Measurements and conceptual insight into factors determining the electrophoretic mobility have been discussed by Hunter [2] and Lyklema [3] and more recently in 2005 publication of IUPAC [4].

Two classes of particles are prominent in electrophoretic mobility studies. The first includes "hard particles" such as rigid spheres with smooth surface. The second class includes "soft particles" with a deformable outer layer. Sarcoplasmic reticulum vesicles – the object of this research - belong to the class of soft particles. Using soft particles as model systems makes possible understanding of surfaces of complex particles and led to the development of applications to stealth liposomes and targeted drug delivery systems [5,6], the understanding of environmental colloid substances [7–9], the relationship between bacterial surface appendages and nanomechanical and electrokinetic properties [10,11] and a series of novel applications such as particles with special magneto-rheological properties [12], coatings that can resist surface fouling by nonspecific protein adsorption [13], and mechanism of biofilm formation [14]. Development of understanding of electrokinetic properties of such particles is of particular interest because of the complexity of their surfaces that often cannot be understood in terms of ζ-potential theory. Instead, treatment of mobility of "soft particles" often requires numerical solutions. In a few select cases analytical or semi-analytical solutions are possible. In these efforts Ohshima is widely recognized for great advancements to the field of electrophoretic mobility of "soft" particles [15–21].

Analytical expressions for mobility play an important role in experimental research. They are very useful in experimental design and development of insight into the electrohydrodynamic properties of the

* Corresponding author.
E-mail address: smejtekp@pdx.edu (P. Smejtek).

0005-2736/$ – see front matter © 2013 Published by Elsevier B.V.
http://dx.doi.org/10.1016/j.bbamem.2013.09.019

surface of particles. These include (a) spherical particles with impermeable core and permeable uncharged surface layer [16], (b) spherical particles with impermeable core and permeable charged surface layer [18], and (c) spherical particles with permeable charged interior without a core [18]. The mobility equation for particles whose major feature is a layer of charge detached from the lipid matrix and embedded in frictional layer, developed in this work, is an important addition to analytical expressions for mobility of soft particles [16,18].

The more complex mobility models that are based on the standard electrokinetic model require numerical solutions. Among the most notable are the models and applications developed in [26] and [27] for soft particles with an uncharged surface layer that were applied to mobility data for phosphatidylglycerol (PG), phosphatidylcholine (PC) with polyethyleneglycol (PEG), and derivatized phosphatidylethanolamine (PE)/phosphatidylcholine(PC) liposomes [28]. The earlier standard electrokinetic models for multilayered soft particles assumed homogeneous layers with sharp boundaries. These were later extended by introducing diffuse boundaries [29,30]. Progress in understanding of electrokinetic processes of microbes has been reviewed recently by Duval and Gaboriaud [11].

The present work is concerned with understanding the processes that determine the electrophoretic mobility of sarcoplasmic reticulum vesicles. Sarcoplasmic reticulum is a membrane envelope present in muscles that concentrates calcium ions by means of Ca pumps (Ca-ATPases), stores these ions, and releases them via Ca-channels in response to arrival of "action potential" signals. SR vesicles are challenging systems because their outer surface is covered with Ca-ATPases protruding from the lipid bilayer matrix (Fig. 1).

Electrokinetic properties of the surface of SR membrane have received marginal attention because the mobility data [22,23] were not interpretable in terms of classic electrokinetic theory based on the notion of ζ-potential [24].

Recently it was shown that the pH-dependence of electrophoretic mobility of SR vesicles is dependent on the pH-dependence of electric charge of APN domains, but not of the whole Ca-ATPase [25]. In that work a linear relationship between the measured electrophoretic mobility and the charge of APN domains originating from ionized amino acid residues was demonstrated.

Here we develop an electrophoretic mobility model whose characteristic feature is a charged plane placed at some distance above the lipid matrix. The plane of charges representing the APN domain (Fig. 1) is embedded within the hydrodynamic frictional layer associated with the layer of calcium pumps at the surface of SR vesicle. It is important that model to be introduced yields an analytical expression for electrophoretic mobility.

The objectives of this work were to explore and to demonstrate the applicability of the "detached charged plane model" to the experimental pH-dependence of mobility of sarcoplasmic reticulum (SR) vesicles. The SR membrane can be regarded as a prototype complex membrane because the charges driving the electrophoretic process are distributed in 3-dimensions at the surface of the vesicle.

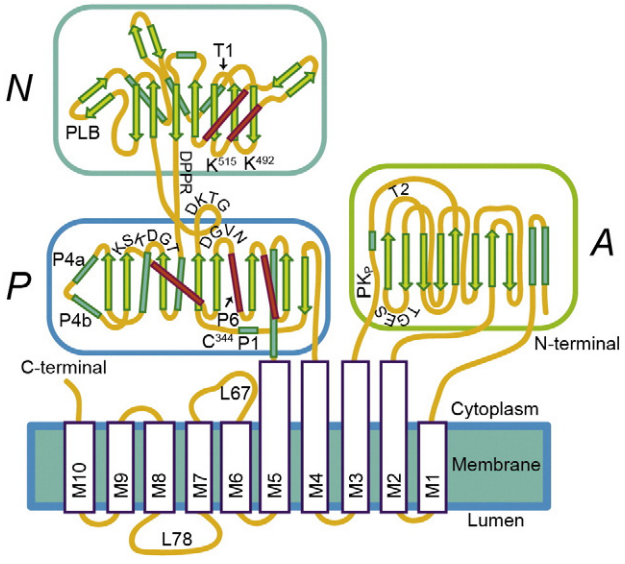

Fig. 1. Basic structure of calcium pump of SR membrane illustrating the A, P, N cytoplasmic domains, and transmembrane helices M. Not to scale. Reproduced with permission from BBA — Biomembranes [25].

2. Materials and methods

SR vesicles were isolated from rabbit fast twitch skeletal muscle by the method of MacLennan [31] and stored in liquid nitrogen. The vesicles were physiologically active. A representative value of the radius of SR vesicles of 130 nm was obtained from particle size distribution [25].

Samples for mobility measurements were prepared by diluting SR vesicles to 0.08 g/L in salt solutions of varying pH and ionic strength. Electrophoretic mobility of SR vesicles was measured at 25 °C using an electrophoretic mobility analyzer DELSA 440 (Beckman–Coulter, Fullerton, CA, USA). Typically, the electrophoretic mobility was measured as a function of ionic strength at six different pH values (4.0, 4.7, 5.0, 6.0, 7.5, and 9.0). For each pH value, the measured mobility data were interpolated to ionic strength of 0.1 M.

The mobility measurements were designed in such a way to obtain reliable mobility data. To reduce the effect of nonrandom errors the mobility data within the range of 50 mM–0.2 M were interpolated to the reference ionic strength of 0.1 M. The reference mobility value at ionic strength of 0.1 M was set for a conceptual reason (see Fig. 3d). To that effect, we have measured the mobility within a region of moderate to high ionic strength, from about 50 mM to 0.2 M, for different pH values. The pH values were 4.0, 4.7, 5.0, 6.0, 7.5, and 9.0 with uncertainty of about 0.1 pH unit. For pH values in the vicinity of mobility reversal it was not possible to obtain mobility data in the full range of ionic strength (0.05 M–0.2 M) because at higher ionic strength the mobility became too small to be reliably measured.

The experimental mobility data collections are summarized in Table 1.

The mobility collection data set represents more than 370 mobility measurements. The data originate from one isolation of SR membranes. There were no significant differences in mobility obtained from different SR isolations. Isolation of SR vesicles was done under the directions of Jon Abramson's on site laboratory to whom we are very grateful.

3. Results

The experimental mobility of sarcoplasmic reticulum vesicles as a function of pH, for ionic strength of 0.1 M of 1:1 salt [25] is shown in Fig. 2. The objective of the present work was to understand the

Table 1
Summary of pH and ionic strength of mobility data collections.

pH	Ionic strength points
4.0	11
4.7	6
5.0	5
6.0	4
7.5	6
9.0	9
Total	41

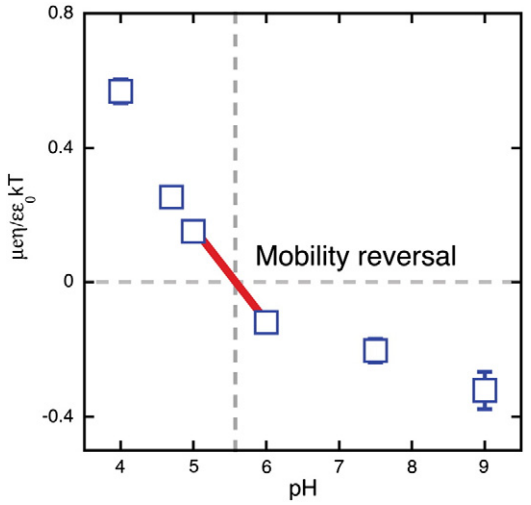

Fig. 2. Dependence of experimental mobility of sarcoplasmic reticulum vesicles on pH, for ionic strength of 0.1 M (1:1) salt [25]. For all points, with the exception of pH 9 the standard deviation of mobility is smaller than the size of the box symbol. The red line indicates the presence of mobility reversal. These experimental data are the basis for understanding of electrohydrodynamic properties of the surface of SR vesicles and the test of the mobility model developed in the paper.

experimental results in terms of the molecular structure of the surface of SR vesicles, vesicle size, and electro-hydrodynamic properties of the surface layer. The mobility data are discussed in terms of a novel model of electrophoretic mobility presented below.

3.1. Detached charged plane (DCP) model for electrophoretic mobility of SR vesicles. The rationale for the DCP model

The rationale for the features of the present DCP model rests on the following properties of the surface of SR: (1) the configuration of APN domains of calcium pump in the "ground", non-pumping state, and (2) the geometry of arrays of calcium pumps at the surface of SR. The rationale is as follows:

Rationale-1: The conformation of calcium pump in the ground state, known as E1, is depicted in Fig. 3a [32]. The A, P, and N domains are spatially extended and are approximately parallel to the surface of the lipid matrix. These domains are represented by a disk located above the surface of the lipid matrix.

Rationale-2: The outer surface of SR vesicles is covered by dense arrays of Ca^{2+}-ATPases with known geometries. It follows from optical diffraction analysis of electron micrographs of freeze-fractured SR vesicles that calcium pumps are self-organized into arrays resembling hexagonal or tetragonal lattices [33]. For tetragonal arrays the dimensions of unit cell are 11.7 ± 0.7 nm in the a-direction and10.5 ± 0.5 nm in the b-direction with unit cell area of 123 ± 9 nm^2. For hexagonal arrays the unit cell defined as body-centered rectangular cell had a repeat distance 13.12 nm, and unit cell area per freeze-fractured particle (the calcium pump) of 130 ± 10 nm^2. In view of these properties the surface of SR vesicles can be visualized as consisting of hexagonal or tetragonal array of disks as depicted in Fig. 3b. Unit cell areas are similar.

Rationale-3: In the DCP mobility model the permeable surface of SR vesicle is represented by a layer containing impermeable spheres with homogeneous volume distribution to produce friction equivalent to that of protruding calcium pumps and by a plane of charge containing the charges of ionizable amino acid residues in APN domains. The details of the surface layer are also shown in Fig. 3c.

Rationale-4: The effect of diffusion polarization can be neglected. This is demonstrated by calculating the dependence of mobility on ionic strength from Smoluchowski model (top curve) and from the standard electrokinetic model [1] (lower curve). It follows from plots in Fig. 3d that for ionic strength of 0.1 M the difference in mobility is negligibly small.

3.2. Electrostatic potential distribution

The electrostatic potential distribution $\psi(x)$ controls the distribution of free ions that drive the electrophoresis. The charged plane positioned at distance s above the lipid matrix separates two regions: Region 1 $0<x<s$, and Region 2 $x>s$.

The electrostatic potential $\psi(x)$ in Region 1 is

$$\psi_1(x) = \frac{\sigma}{2\varepsilon\varepsilon_0\kappa}[\exp(-\kappa(s-x)) + \exp(-\kappa(s+x))] \quad (1)$$

and in Region 2 is

$$\psi_2(x) = \frac{\sigma}{2\varepsilon\varepsilon_0\kappa}[\exp(\kappa(s-x)) + \exp(-\kappa(s+x))]. \quad (2)$$

σ is the charge density of the plane and κ is the Debye–Hückel parameter (the reciprocal thickness of the electric double layer surrounding the charged plane).

$$\kappa = \left(\frac{F^2 2000\,(IS)}{\varepsilon\varepsilon_0 RT}\right)^{1/2} \quad (3)$$

Ionic strength, *IS*, and other quantities have their usual meaning.

3.3. Velocity of electroosmotic flow and the mobility of SR vesicles

The mobility of the particle is obtained from the distribution of velocity of electroosmotic flow of fluid around the particle $u(x)$ that follows from the Navier–Stokes–Brinkman equation

$$\frac{d^2u(x)}{dx^2} - \lambda^2 u(x) + \frac{\rho_{mob}(x)\,E_{appl}}{\eta} = 0. \quad (4)$$

The second term in Eq. (4) is proportional to the retarding force exerted by friction in the surface layer representing the layer of calcium pumps. The third term is proportional to the electric force driving the flow of solution by the applied electric field.

In the DCP model, the second term of Eq. (4) originates from resistance centers, each producing retarding force, f_S. For a stationary particle f_S is proportional to the local velocity of flow of the solution, u,

$$f_S = 6\pi a_S \eta u \quad (5)$$

a_S is the radius of Stokes resistance center (Einstein's impermeable sphere), and η the viscosity coefficient. The frictional coefficient per unit volume of a surface layer containing N_S Stokes resistance centers is

$$\gamma = 6\pi a_S \eta N_S. \quad (6)$$

The softness parameter of particle surface layer, λ, is equal to

$$\lambda = \sqrt{\frac{\gamma}{\eta}}. \quad (7)$$

Its reciprocal value, λ^{-1}, is known as the Debye–Bueche length or the flow penetration depth.

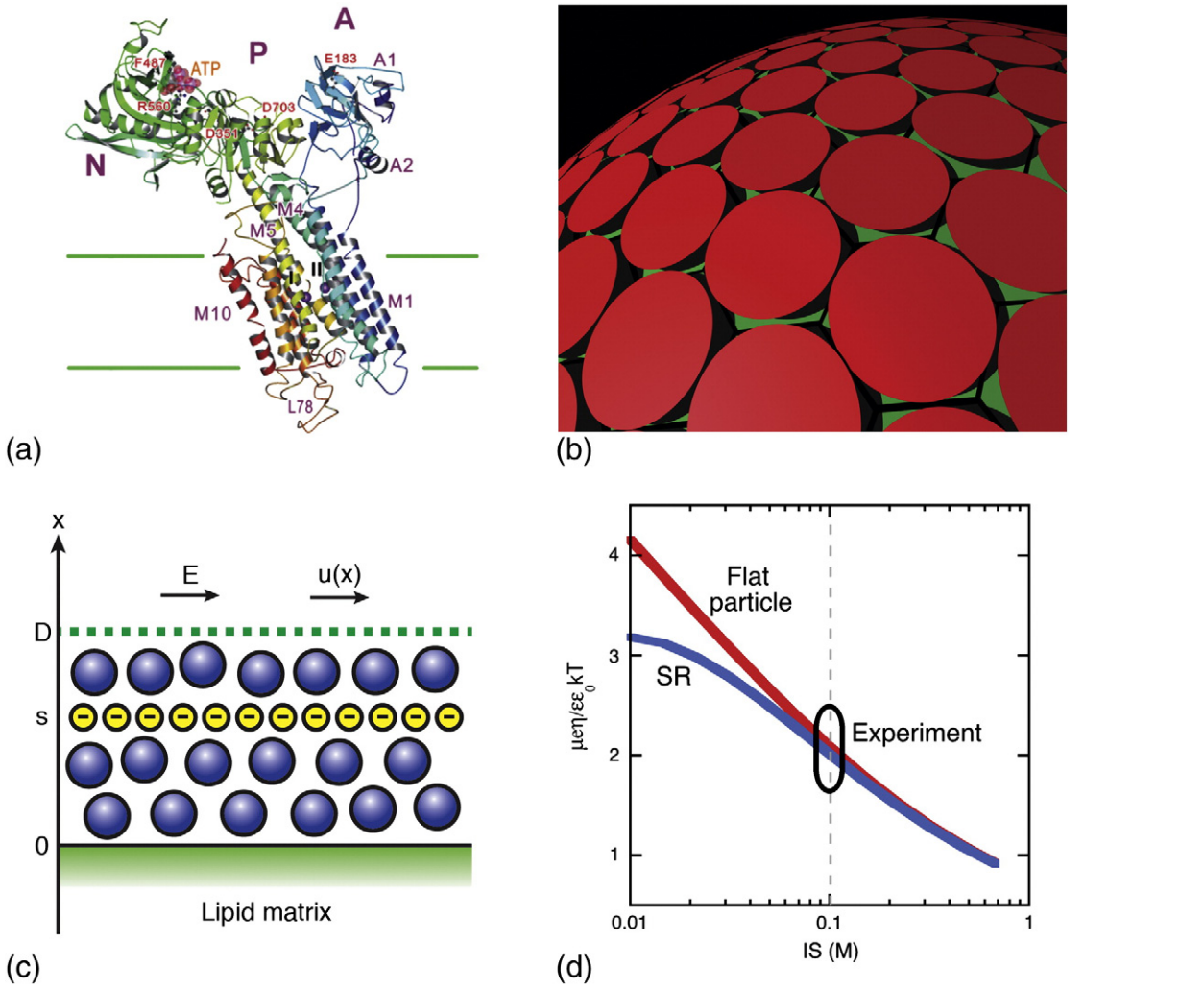

Fig. 3. a: Due to the translational and rotational diffusion, the A, P, and N domains can be visualized as disks located above the surface of the lipid matrix. Reproduced with permission from Archives of Biochemistry and Biophysics [32]. b: Surface of SR vesicles is visualized as consisting of hexagonal or tetragonal array of disks. c: The surface of SR vesicles is covered by dense array of Ca^{2+}-ATPases (calcium pumps). The protruding calcium pumps introduce hydrodynamic drag on the solution flowing through the surface layer of SR vesicle. In the model, the frictional effect due to the calcium pumps is accounted for by the presence of Einstein's impermeable spheres within the surface layer of thickness D. The position of charged plane is denoted by s; σ is the charge density of the charged plane. The external electric field E_{appl} drives the electroosmotic flow $u(x)$. d: Effect of double layer polarization on mobility. Plots of dimensionless mobility vs ionic strength computed from the Smoluchowski model in which the polarization effect is absent (top curve), and from the general electrokinetic model in which the polarization is present (lower curve). In both cases we consider bare particles without frictional layer. The particle surface charge density, $\sigma(pH4) = 0.0107$ As-m^{-2}, was that of SR vesicles at pH 4. For the top curve the particle radius was assumed to be infinity, whereas for the lower curve it was 130 nm, a typical value for SR liposomes used in the study. Ionic strength of liposome suspension was 0.1 M. Due to small difference between mobility, the diffusion polarization effects can be ignored in this work.

The velocity of electroosmotic flow is characterized by three regions: Region 1 $0<x<s$, Region 2 $s<x<D$ and Region 3 $D<x$. The solution for the mobility is set up relative to the surface of the lipid matrix fixed in space. The flow of aqueous phase above the lipid matrix of SR is driven by the external electric field applied parallel to the surface, E_{appl}. The velocity of electroosmotic flow at the surface is zero because the aqueous phase adheres to the surface of the core. The magnitude of velocity increases for $x>0$, and reaches a constant value as $x \to \infty$. The velocity of electroosmotic flow at infinity is designated by u_{EO}.

In the electrophoretic mobility experiment the situation is opposite, the particle is free and it moves relative to the solution in opposite direction with velocity $-u_{EO}$ (note: In the electrophoretic mobility experiment the velocity of flow of aqueous phase is zero. In view of this geometry the electrophoretic mobility of the free particle is

$$\mu = -\frac{u_{EO}}{E_{appl}}. \tag{8}$$

E_{appl} is the external electric field applied to the vesicle.

The mobility of DCP particles obtained from Eq. (8) is

$$\mu_{DCP} = \mu_0 \frac{\kappa^2}{\kappa^2 - \lambda^2} \left\{ \begin{array}{l} \frac{1}{\cosh(\lambda D)} \left[\exp(-\kappa s) + \left(\frac{\kappa}{\lambda}\right) \sinh(\lambda s) \right] - \\ -\left(\frac{\lambda}{\kappa}\right) \cosh(\kappa s) \exp(-\kappa D) \left[tanh(\lambda D) + \left(\frac{\lambda}{\kappa}\right) \right] \end{array} \right\}. \tag{9}$$

The term μ_0 in Eq. (9) can be regarded as the mobility of a similar but bare particle. One lacking the frictional layer and having the charge of the detached charged plane located at the particle surface. The mobility of the bare particle with surface charge equal to that of the detached charged plane is

$$\mu_0 = \frac{\sigma}{\eta\kappa}. \tag{10}$$

The mobility ratio μ_{DCP}/μ_0 defines the mobility structure factor, $MSF(s, D, \lambda, \kappa)$. MSF reflects the properties of the surface layer of SR

vesicle: the position of charged plane s, the thickness of the frictional layer D, and the particle softness λ.

$$MSF(s,D,\lambda,\kappa) = \frac{\kappa^2}{\kappa^2-\lambda^2}\left\{\begin{array}{l}\frac{1}{\cosh(\lambda D)}\left[\exp(-\kappa s)+\left(\frac{\kappa}{\lambda}\right)\sinh(\lambda s)\right]- \\ -\left(\frac{\lambda}{\kappa}\right)\cosh(\kappa s)\exp(-\kappa D)\left[tanh(\lambda D)+\left(\frac{\lambda}{\kappa}\right)\right]\end{array}\right\}. \quad (11)$$

In condensed form, the mobility of particles of this type has a simple form,

$$\mu_{DCP} = \mu_0 MSF(s,D,\lambda,\kappa). \quad (12)$$

Alternatively to the Debye Bueche length, the frictional properties of the surface layer of SR vesicles can be characterized by the dimensionless retardation index

$$RI = \frac{\lambda}{\kappa}. \quad (13)$$

RI is the ratio of the Debye length (κ^{-1}) to the Debye–Bueche length (λ^{-1}).

3.4. The effect of the position of charged plane on mobility

The dependence of mobility structure factor, $MSF(s, D, \lambda, \kappa)$, on the position of the charged plane as a function of retardation index, RI, is illustrated in Fig. 4. The top curve is for frictionless coating, $RI = 0$. In the absence of retardation MSF changes from unity when the charged plane coincides with the surface of particle core, to $MSF = 5.704$ for charged plane at the top of the coating ($D = 10$ nm). This demonstrates the effect of position of charged plane on the mobility of particle, viz the mobility of frictionless particle with detached charged plane would increase 5.704 times relative to the mobility of frictionless hard particle due to charges being moved to 10 nm above the lipid matrix. The lower broken curves are plots of MSF for a stepwise increase of retardation index by 0.25. The notable feature of the DCP model is that for charged plane close to the particle core, the MSF, and thus the mobility, decrease with RI more rapidly than for a charged plane close to the top of the coating. This means that the sensitivity of mobility to the position of charged plane is greater for particles with greater retardation.

4. Application of DCP model to SR vesicles

4.1. Electric charge of APN domains and its dependence on pH

The A, P, and N domains of the Ca^{2+}-ATPase were defined by Reuter, Hinsen, and Lacapere [34]. The APN domains are simply the combination of these three domains. The electric charge of APN domains is determined by the ionizable side chain of amino acid residues. The composition and number of amino acids in each domain were obtained from Fig. 5 of the paper by Shi, Chen, Huvos, and Hardwicke [35]. The ionizable amino acid residues, their polarity, pKa values and their frequencies of occurrence are listed in Table 2.

The charge density of APN plane in the mobility model, σ_{APN}, is obtained from the assumption that the charge of APN domains, Q_{APN}, is spread over the area of unit cell of calcium pump arrays, A_{uc}, at the surface of SR vesicles (Fig. 2). The charge of APN domains is

$$Q_{APN} = Q_A + Q_P + Q_N = \\ = eh_{A,i}\left(p_{A,i}, pH, \psi_{A,i}\right) + eh_{P,i}\left(p_{P,i}, pH, \psi_{P,i}\right) + eh_{N,i}\left(p_{N,i}, pH, \psi_{N,i}\right). \quad (14)$$

The ionization function of amino acid of type i listed in Table 2, h_i, depends on the bulk pH and the local electrostatic potential at the protolytic site, ψ_i.

$$h_i(p_i, pH, \psi_i) = \frac{1}{1 + 10^{p_i(pH-pKa_i)}\cdot\exp\left(p_i\frac{F\psi_i}{RT}\right)}. \quad (15)$$

p_i is the polarity index in Table 2.

We consider tetragonal arrays of calcium pumps with unit cell area of 123 ± 9 nm^2 [33]. The charge density of the DCP plane depends on the charge of APN domain, Q_{APN}, and the unit cell area, A_{UC}.

$$\sigma_{APN} = \frac{Q_{APN}}{A_{uc}}. \quad (16)$$

In the mobility analysis below the electrostatically induced pH correction was not included for several reasons, (a) the protolytic sites on APN domains are discrete sites and are not exposed to "averaged" electrostatic potential of the charged plane, (b) the mobility study was done at ionic strength of 0.1 M corresponding to short Debye length of

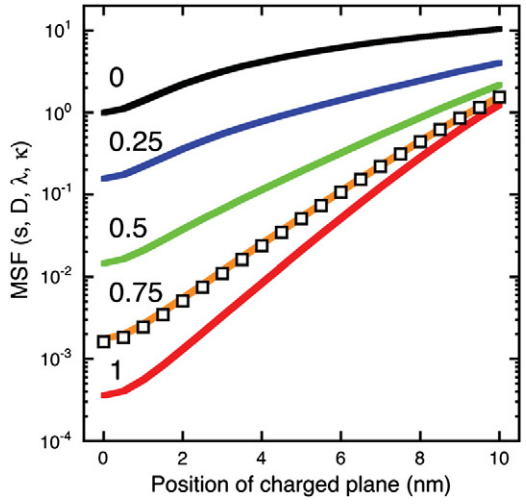

Fig. 4. The dependence of mobility structure factor, $MSF(s, D, \lambda, \kappa)$, on the position of the charged plane as a function of retardation index, RI. The top curve is for frictionless coating $RI = 0$. Lower curves RI: 0.25, 0.5, 0.75, 1.0. The MSF data points are for $RI = 0.762$ corresponding to the fit of the DCP model to the measured mobility vs pH shown in Fig. 8.

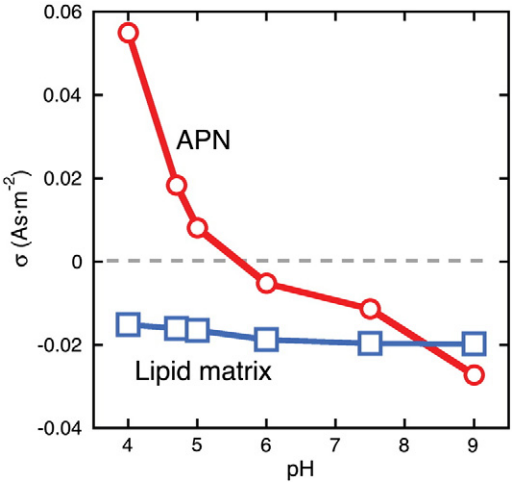

Fig. 5. Charge density of APN domain (top curve) and lipid matrix (lower curve) computed for ionized amino acid residues present in Ca^{2+}-ATPase (calcium pump) and charged lipids of lipid matrix. Charge density of APN domain was computed for amino acids listed in Table 2 and those of lipid matrix for lipids listed in Table 3.

Table 2
Amino acids in A, P, and N domains of Ca^{2+}-ATPase (calcium pump). The quantities in columns are the number of each amino acid residues; the polarity of their charged form and selected pKa values are for amino acid residues in polypeptides.

Amino acid	Polarity	pKa	A	P	N
Arginine	+1	12.2	9	9	15
Aspartic acid	−1	4.0	10	10	14
Cysteine	−1	8.7	1	7	8
Glutamic acid	−1	4.3	12	13	19
Histidine	+1	6.4	4	0	0
Lysine	+1	10.5	13	7	17
Tyrosine	−1	9.8	3	2	5

Values from Jack Kyte, Structure in Protein Chemistry, Garland Publishing, 1995.

0.96 nm, and (c) forcing the electrostatic pH correction destroys the agreement of the computed and measured pH dependence of mobility.

4.2. Electric charge of the lipid matrix and its dependence on pH

Negative charges of lipid matrix of SR vesicles are due to phosphatidylinositol (7.6%) and phosphatidylserine (2%) [36]. Assuming 0.7 nm^2 of membrane surface area per lipid, tetragonal unit cell area of 123 nm^2 and subtracting 12.6 nm^2 for the stalk of the Ca^{2+}-ATPase, we found that there are 12 PI and 3.15 PS molecules per Ca^{2+}-ATPase unit cell.

The charge due to lipids per unit cell of Ca^{2+}ATPase is

$$Q_{LM} = Q_{PI} + Q_{PS1} + Q_{PS2} + Q_{PS3} = eh_{PI}(p_{PI}, pH, \psi_{PI}) + \\ + eh_{PS,1}\left(p_{PS,1}, pH, \psi_{PS,1}\right) + eh_{PS,2}\left(p_{PS,2}, pH, \psi_{PS,2}\right) + eh_{PS,3}\left(p_{PS,3}, pH, \psi_{PS,3}\right). \quad (17)$$

The surface charge density of lipid matrix is

$$\sigma_{LM} = \frac{Q_{LM}}{A_{uc}}. \quad (18)$$

4.3. WSDSQ — weighted sum of mobility deviation squared

There are two types of contribution to "theoretical" mobility, one from the lipid matrix, and one from APN domains,

$$\mu_{LM}(\sigma_{LM}, 0, D, \lambda, \kappa) = \frac{\sigma_{LM}}{\eta\kappa} MSF(0, D, \lambda, \kappa) \\ \mu_{APN}(\sigma_{APN}, s, D, \lambda, \kappa) = \frac{\sigma_{APN}}{\eta\kappa} MSF(s, D, \lambda, \kappa). \quad (19)$$

Mobility structure factor $MSF(0, D, \lambda, \kappa)$ applies to the lipid matrix ($s = 0$) and $MSF(s, D, \lambda, \kappa)$ to APN domains ($s > 0$).

The applicability of the DCP model is evaluated using the weighted sum of deviation squared, *WSDSQ*,

$$WSDSQ = \frac{1}{p_{\max}} \sum_p \frac{\left[\mu x_p - (\mu_{LM}(\sigma_{LM}, 0, D, \lambda, \kappa) + \mu_{APN}(\sigma_{APN}, s, D, \lambda, \kappa))\right]^2}{sd\mu x_p^2}. \quad (20)$$

In Eq. (20) p is the index of experimental mobility point μx, μx_p the experimental mobility value, $sd\mu x_p$ the standard deviation of experimental mobility point μx_p, σ_{LM} the charge density of lipid matrix, σ_{APN} the charge density of APN domains, s the position of APN plane, D the thickness of Ca pump surface layer, λ the softness parameter of surface layer and κ the Debye–Hückel parameter.

Our interest is to develop insight into how the Debye Bueche length, λ^{-1}, (and corresponding softness λ) of the surface layer and the position of APN domain plane affect the value of *WSDSQ* and thus the degree of fit of the DCP model to the mobility data. To accomplish this, a set of Debye Bueche lengths was selected and *WSDSQ* obtained from Eq. (20).

Table 3
Charges in lipid matrix of SR.

Lipid	Polarity	pKa	N/unit cell
PS phosphate deprotonation (POH)	−1	2.6	3.15
PS carboxyl deprotonation (COOH)	−1	5.5	3.15
PS amino deprotonation (NH^{3+})	+1	11.55	3.15
PI phosphate deprotonation (POH)	−1	2.5	12

The plots of *WSDSQ* for individual Debye Bueche lengths (and retardation indices) are illustrated below. The leftmost curve corresponds to the longest Debye Bueche length and a smallest retardation index, the rightmost one is for the shortest Debye Bueche length and greatest retardation index. The minimum values of the *WSDSQ* for each retardation index determine the best fit values for the position of the plane of charge representing the APN domain. Data in Fig. 5 map the properties of *WSDSQ* surface. Five branches of *WSDSQ* were obtained for the five preset values of the Debye Bueche length listed in Table 4.

There is one minimum value of *WSDSQ* present for each branch. The plots of *WSDSQ* show that position of APN domain and *WSDSQ* correlate, the minimum *WSDSQ* depends not only on the position of the APN domain, s, but also on the Debye Bueche length (Fig. 6). The magnitude of *WSDSQ* at the minimum depends on the position of APN domain within the surface layer of SR.

Until now there was no explicit information on where the APN domain may be located, and how it is related to the mobility. These issues are addressed in Fig. 7.

As noted earlier the minimum value of *WSDSQ* depends on the position of APN domain within the surface layer. The relationship between the value of *WSDSQ* minimum (best fit) and the location of APN domain is depicted in Fig. 7. It follows from the plot that better agreement between the mobility predicted from the DCP model and the experimental results takes place when APN domain is located in the upper half of the surface layer of SR vesicles. This observation is supported by the molecular structure of the Ca^{2+}-ATPase (Fig. 1). The plot illustrates that the experimental mobility of SR vesicles can be understood in terms of the DCP mobility model.

4.4. Dependence of DCP mobility on pH

The dependence of measured and theoretical mobility on pH is compared in Fig. 8. The theoretical mobility included the pH-dependent charge density of lipid matrix and that of APN domains predicted from the amino acid sequence of calcium pumps. The solid curve was obtained by interpolation.

This work is also an illustration of how a biophysical model provides insight into the coupling of electrostatic potential and electroosmotic flow velocity distributions. The analytical solution of mobility was derived from solving a set of boundary conditions for the electrostatic and hydrodynamic properties of the surface of SR vesicles. The agreement between the experimental and theoretical mobility shown in Fig. 8 confirmed the validity of the rationale invoked in the design of

Table 4
Set of Debye Bueche lengths and softness of surface layer of SR vesicles used to evaluate *WSDSQ*.

Debye Bueche length λ^{-1} (nm)	Softness of surface layer λ (m^{-1})	Retardation index
3.15	320×10^6	0.305
2.54	394×10^6	0.378
2.01	498×10^6	0.477
1.46	685×10^6	0.657
0.802	1250×10^6	1.2

Note: High softness parameter corresponds to short Debye Bueche length.

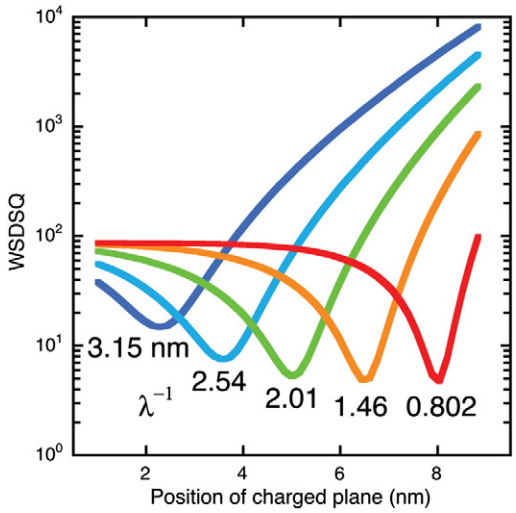

Fig. 6. Plots of "weighted sum of deviation squared", *WSDSQ*, given by Eq. (20) as a function of the position of APN plane for preset values of the Debye Bueche length of the surface layer. Plots show that position of APN plane and *WSDSQ* correlate, the minimum *WSDSQ* depends not only on the position of charged plane, *s*, but also on the Debye Bueche length (λ^{-1}). Note that *WSDSQ* decreases as the APN plane position within the surface layer increases.

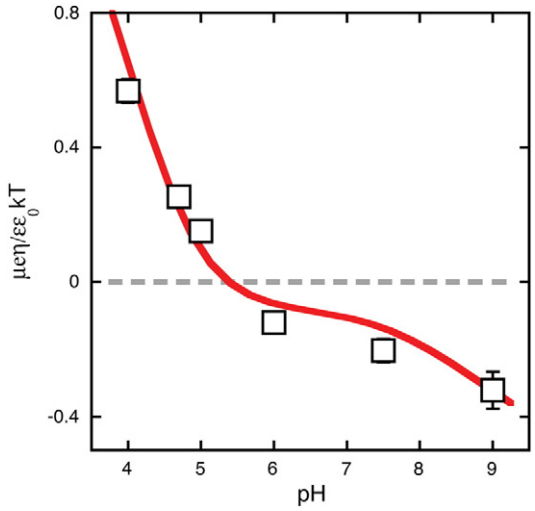

Fig. 8. The dependence of measured and theoretical mobility of SR vesicles on pH. The theoretical mobility was obtained from the DCP model including the pH-dependent charge density of lipid matrix and that of APN domains as predicted from the amino acid sequence of calcium pumps. The solid curve illustrates the DCP model mobility obtained by interpolating the optimum theoretical mobility results. The theoretical pH-dependence of mobility was calculated for a position of APN domains 7 nm above the lipid matrix, within the surface layer of calcium pumps of assumed thickness of 10 nm. The optimum value of the Debye Bueche length (λ^{-1}) corresponding to the minimum of "weighted sum of deviation squared" was 1.26 nm.

the DCP mobility model. The DCP model developed here complements simple mobility models of soft particles [16,18,19].

The DCP model illuminates the origin of mobility increase with increasing *s*, and the mobility attenuation with decreasing Debye Bueche length, λ^{-1}. These two quantities along with the pH-dependent charge densities of amino acid residues of APN domains and the ionizable lipids of the lipid matrix are the major components associating the DCP model with the molecular properties of the SR surface. The DCP model developed here complements simple mobility models of soft particles [16,18,19].

5. Conclusions

Sarcoplasmic reticulum membrane (SR) was regarded here as a prototype complex biomembrane due to the presence of Ca^{2+}-ATPases (calcium pumps) at the outer surface of SR vesicles. The surface of SR vesicles is charged due to charged lipids present in the lipid matrix and due to charges originating from the Ca^{2+}-ATPases. It was not clear how these charges influence the flow of free ions surrounding the SR membrane that determine the electrohydrodynamic properties of SR vesicles. This issue was investigated here experimentally by measuring the velocity of SR vesicles in an external electric field.

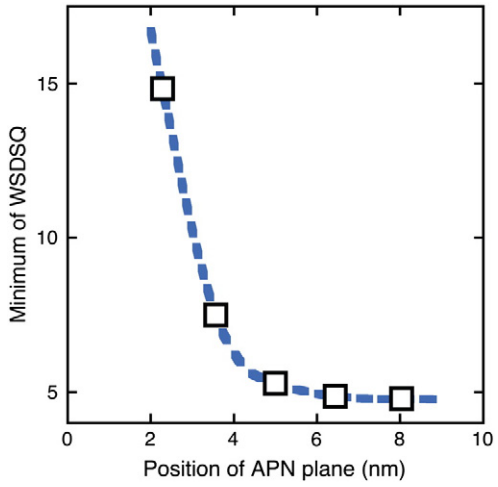

Fig. 7. Relationship between the value of "weighted sum of deviation squared minimum", *WSDSQ*, and the position of APN domain within the surface layer. The plot illustrates that better agreement between the DCP model and the experimental dependence of mobility on pH takes place for APN plane located in the upper half of the surface layer of calcium pumps. The broken curve relating the value of *WSDSQ* minimum to the position of APN plane was obtained by interpolation.

The electrophoretic mobility is determined by forces both driving and retarding the motion of SR vesicles. The mobility depends on charges present at the surface of the lipid matrix, charges of the Ca^{2+}-ATPases embedded in the lipid matrix and the frictional effect of the layer of Ca^{2+}-ATPases at the outer surface of SR vesicles. An analytical solution for mobility was derived by solving a set of boundary conditions for the electrostatic and hydrodynamic properties of the surface of SR vesicles (see Appendix A).

Since the lipid composition of the lipid matrix is known it was possible to predict the pH-dependence of electric charge density of the lipid matrix. Similarly, the effect of pH on ionizable amino acid residues of APN domains of the ATP-ases was also evaluated because the amino acid sequence of the ATP-ase and the ionization properties of amino acid residues are known. What was not known, and had to be established, was the effect of electric charges distributed in 3-dimensions at the surface of SR vesicles. In addition to accounting for the effect of driving electric force it was necessary to account for the hydrodynamic friction introduced by Ca^{2+}-ATPases within the outer surface of SR vesicles. These were the general concepts explored in this work.

We have shown that it is possible to understand the pH-dependence of mobility of SR vesicles in terms of a simple biophysical model of the surface of SR membrane, the DCP model. It was also shown how the mobility of SR vesicles was determined by the charges present in APN domains of Ca^{2+}-ATPases. These domains were represented in the DCP model by a charged plane detached from the lipid matrix and immersed in the frictional layer. Another charged plane included in the model was associated with charged lipids of the lipid matrix of SR vesicles.

From the interpretation of the measured pH-dependence of mobility of SR vesicles it was concluded that charges of lipid matrix make a very small contribution to the mobility of SR vesicles. The major contribution

was primarily determined by charges of APN domains. It also followed from the DCP model that the contribution APN domains to mobility is enhanced by their location above the lipid matrix. The DCP model also explained why the contribution of charged lipid matrix to mobility of SR vesicles was suppressed.

The successful interpretation of mobility data of SR vesicles in terms of the DCP model and the ability to develop an analytical solution for the mobility of SR vesicles followed from the reduction of complexity of the electrohydrodynamic structure of the surface of SR vesicles. The driving force was associated with the charges of APN domains of the Ca^{2+}-ATPases and of charged lipid matrix. Both sets of charges were pH-dependent. The retarding force due to the forest of Ca^{2+}-ATPases was represented by an uncharged homogeneous frictional layer producing the same retarding effect as the layer of Ca^{2+}-ATPases protruding from the outer surface of the lipid matrix of SR (Fig. 3a, b, c).

The mobility equation for particles whose major feature is a layer of charge detached from the lipid matrix and embedded in frictional layer, developed in this work (Eq. (9)), is an important addition to analytical expressions for mobility of soft particles [16,18].

Acknowledgements

We appreciate the support from the Physics Department of Portland State University. Also, we would like to acknowledge the contribution of the following faculty Jon Abramson, Kwan Hsu and Arnold Pickar to the development of membrane biophysics research in Physics Department.

Appendix A. Electrostatic potential and electroosmotic velocity distribution for SR vesicles

A1. Electrostatic potential distribution

There are two electrostatic regions, separated by the charged plane at $x = s$, where the solution of linearized Poisson–Boltzmann equation

$$\frac{d^2\psi(x)}{dx^2} = \kappa^2\psi(x) \tag{A1}$$

is required:

Region 1, $0 < x \le s$

$$\psi_1(x) = A\exp(\kappa x) + B\exp(-\kappa x). \tag{A2}$$

Region 2, $x > s$

$$\psi_2(x) = C\exp(-\kappa x) + D\exp(\kappa x). \tag{A3}$$

From conventional electrostatic boundary conditions follows the distribution of electrostatic potential,
in Region 1

$$\psi_1(x) = \frac{\sigma}{2\varepsilon\varepsilon_0\kappa}[\exp(-\kappa(s-x)) + \exp(-\kappa(s+x))] \tag{A4}$$

and in Region 2

$$\psi_2(x) = \frac{\sigma}{2\varepsilon\varepsilon_0\kappa}[\exp(\kappa(s-x)) + \exp(-\kappa(s+x))]. \tag{A5}$$

A2. Solution for the velocity of electroosmotic flow

To obtain the velocity distribution of electroosmotic flow the Navier–Stokes–Brinkman equation is solved in three regions. Within the surface layer we have:Region 1, $0 < x \le s$

$$\frac{d^2u_1(x)}{dx^2} - \lambda^2 u_1(x) = \frac{\varepsilon\varepsilon_0\kappa^2 E_{appl}}{\eta}\psi_1(x) \tag{A6}$$

and Region 2, $s \le x \le D$

$$\frac{d^2u_2(x)}{dx^2} - \lambda^2 u_2(x) = \frac{\varepsilon\varepsilon_0\kappa^2 E_{appl}}{\eta}\psi_2(x). \tag{A7}$$

The hydrodynamics of the particle surface layer follows from the Debye–Bueche approach. The coating is represented by an array of frictional centers. It is characterized by the hydrodynamic penetration depth, λ^{-1}, also known as the Debye Bueche length. Quantity λ is a measure of hydrodynamic softness of the surface layer composed of calcium pumps.

Region 3, $x > D$, where the surface layer is absent, and the electrostatic potential is $\psi_2(x)$

$$\frac{d^2u_3(x)}{dx^2} = \frac{\varepsilon\varepsilon_0\kappa^2 E_{appl}}{\eta}\psi_2(x). \tag{A8}$$

The general solutions for velocity of flow are:
in Region 1

$$u_1(x) = F\exp(\lambda x) + G\exp(-\lambda x) + \\ + \frac{\sigma\kappa}{2\eta(\kappa^2-\lambda^2)}E_{appl}\{\exp[-\kappa(s-x)] + \exp[-\kappa(s+x)]\} \tag{A9}$$

in Region 2

$$u_2(x) = K\exp(\lambda x) + L\exp(-\lambda x) + \\ + \frac{\sigma\kappa}{2\eta(\kappa^2-\lambda^2)}E_{appl}\{\exp[-\kappa(x-s)] + \exp[-\kappa(x+s)]\} \tag{A10}$$

and in Region 3

$$u_3(x) = u_{EO} + \frac{\sigma E_{appl}}{2\eta\kappa}\{\exp[-\kappa(x-s)] + \exp[-\kappa(x+s)]\}. \tag{A11}$$

A3. Boundary conditions for the electroosmotic flow

Fluid boundary condition at the surface of the particle core (FBC1)

Applying the condition of zero velocity at $x = 0$, $u_1(0) = 0$ to Eq. (A8) results in

$$F + G + \frac{\sigma\kappa}{\eta(\kappa^2-\lambda^2)}E_{appl}\exp(-\kappa s) = 0. \tag{A12}$$

Fluid boundary condition at the charged plane (FBC2)

Applying the condition of continuity of velocity at $x = s$, $u_1(s) = u_2(s)$ results in

$$F\exp(\lambda s) + G\exp(-\lambda s) - K\exp(\lambda s) - L\exp(-\lambda s) = 0. \tag{A13}$$

Fluid boundary condition at the charged plane (FBC3)

Applying the condition of continuity of first derivative of velocity at $x = s$, $du_1/dx = du_2/dx$, requires that

$$F\exp(\lambda s) - G\exp(-\lambda s) - K\exp(\lambda s) + L\exp(-\lambda s) \\ = -\frac{\sigma\kappa^2}{\eta\lambda(\kappa^2-\lambda^2)}E_{appl}. \tag{A14}$$

Fluid boundary condition at the interface between the frictional layer and free solution (FBC4)

Applying the condition of continuity of velocity at $x = D$, $u_2(D) = u_3(D)$, results in

$$K\exp(\lambda D) - L\exp(-\lambda D) = \\ = \frac{\lambda}{(\kappa^2-\lambda^2)}\frac{\sigma E_{appl}}{2\eta}\{\exp[-\kappa(D-s)] + \exp[-\kappa(D+s)]\}. \tag{A15}$$

Fluid boundary condition at the interface between the frictional layer and free solution (FBC5)

Applying the condition of continuity of first derivative of velocity at $x = D$, $du_2/dx = du_3/dx$ requires that

$$K\exp(\lambda D) - L\exp(-\lambda D) = \\ = \frac{\lambda}{(\kappa^2-\lambda^2)}\frac{\sigma E_{appl}}{2\eta}\{\exp[-\kappa(D-s)] + \exp[-\kappa(D+s)]\}. \quad (A16)$$

A4. Velocity distribution of electroosmotic flow

The velocity distributions inside the frictional layer depend on constants *F*, *G*, *K*, and *L*. These quantities are

$$K = \frac{1}{2}u_{EO}\exp(-\lambda D) + \frac{\sigma E_{appl}}{2\kappa\eta}\left(1-\frac{\lambda}{\kappa}\right) \\ \times\left(\frac{\kappa\lambda}{\kappa^2-\lambda^2}\right)\cosh(\kappa s)\exp(-\kappa D)\exp(-\lambda D) \quad (A17)$$

$$L = \frac{1}{2}u_{EO}\exp(\lambda D) - \frac{\sigma E_{appl}}{2\kappa\eta}\left(1+\frac{\lambda}{\kappa}\right) \\ \times\left(\frac{\kappa\lambda}{\kappa^2-\lambda^2}\right)\cosh(\kappa s)\exp(-\kappa D)\exp(\lambda D) \quad (A18)$$

$$G = -K\frac{\exp(\lambda s)}{2\sinh(\lambda s)} - L\frac{\exp(-\lambda s)}{2\sinh(\lambda s)} - \frac{\sigma E_{appl}}{\kappa\eta}\frac{\kappa^2}{\kappa^2-\lambda^2}\exp(-\kappa s)\frac{\exp(\lambda s)}{2\sinh(\lambda s)} \quad (A19)$$

$$F = -G - \frac{\sigma E_{appl}}{\kappa\eta}\frac{\kappa^2}{\kappa^2-\lambda^2}\exp(-\kappa s). \quad (A20)$$

The position of the charged plane relative to the surface of the particle core determines the distribution of electrostatic potential, which in turn determines the distribution of density of mobile ions in the electrical double layer and the distribution of velocity of electroosmotic flow. The mobility of particles is determined from the velocity of electroosmotic flow far from the surface of frictional layer u_{E0} according to Eq. (8).

Fig. A1a illustrates the effects of the position of the charged plane on the electrostatic potential distributions $\psi(x)$ (Fig A1a) and the

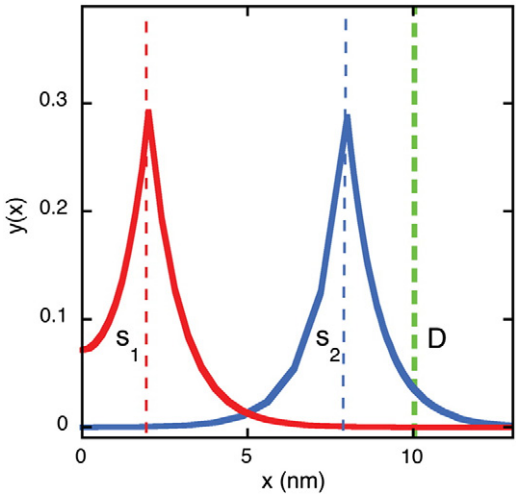

Fig. A1a. Dimensionless potential distribution, $y(x) = e\psi(x)/kT$, in the surface layer for deep (2 nm) and shallow (8 nm) APN plane. The plots of $y(x)$ were obtained for ionic strength 0.1 M and charge density of APN plane of $\sigma_{APN} = 0.0107$ As-m^{-2} corresponding to SR vesicle mobility at pH 4. Thickness of surface layer $D = 10$ nm.

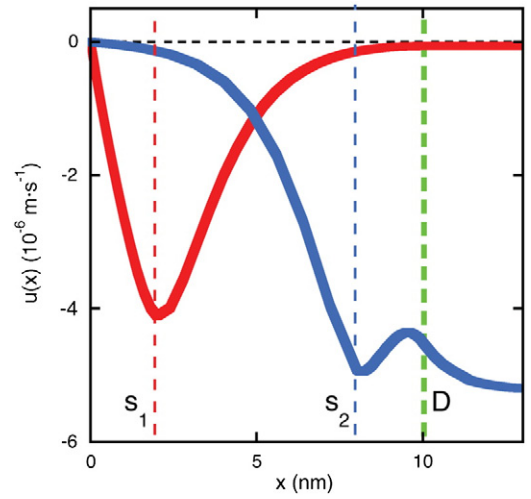

Fig. A1b. Distribution of electroosmotic flow velocity, $u(x)$, within and outside of the surface layer for deep (2 nm) and shallow (8 nm) APN plane. The external applied electric field $E_{appl} = 1000$ V-m^{-1}, other quantities are given in Fig. A1a.

electroosmotic velocity flow distributions $u(x)$ (Fig A1b) for a frictional layer of thickness $D = 10$ nm characterized by a Debye–Bueche length $\lambda^{-1} = 1.28$ nm. In this illustration the solution is for ionic strength 0.1 M the value of the Debye length $\kappa^{-1} = 0.961$ nm. These conditions define the retardation index $RI = 0.75$.

The electrostatic potential distributions were computed for surface charge density of APN plane $\sigma = 0.0107$ As-m^{-2} corresponding to mobility at pH 4. The distribution of velocity of electroosmotic flow, $u(x)$, was obtained using constants *F*, *G*, *K*, and *L* defined by Eqs. ((A17)–(20)).

Two positions of the charged plane were considered, one close to the surface of the core, $s_1 = 2$ nm, and one close to the top of frictional layer, $s_2 = 8$ nm. For the charged plane at s_1 the electrical double layer is confined to the frictional layer, whereas for the charged plane at s_2 the electrical double layer partially extends beyond the frictional layer.

The position of the charged plane has a great effect on the velocity distributions and mobility of particles. To illustrate the effect, the dimensionless mobility of vesicles with APN plane at $s_1 = 2$ nm was $\mu_1 = 3.17 \times 10^{-3}$ whereas mobility of those with APN plane at $s_2 = 8$ nm was substantially greater, $\mu_2 = 0.260$.

There are two main physical contributions to this difference. The first originates from the no-slip condition at the vesicle surface. Since screening charges drive the electroosmotic flow, their spatial distribution determines the flow velocity profile. In the case of s_1, greater concentrations of screening charges are present close to the particle core surface, an area of suppressed flow due to proximity to the no slip boundary. The second contribution resulting in a higher value of μ_2, is that the space charge of screening ions surrounding the APN plane at s_2 extends beyond the boundary of the frictional surface layer.

References

[1] R.W. O'Brien, L.R. White, Electrophoretic mobility of a spheroidal colloidal particle, J. Chem. Soc. Faraday Trans. 2 (74) (1978) 1607–1626.
[2] R.J. Hunter, Zeta Potential in Colloid Science, Academic Press, 1981.
[3] J. Lyklema, Fundamentals of Interface and Colloid Science, Academic Press, London, San Diego, 1995.
[4] A.V. Delgado, F. Gonzalez-Caballero, R.J. Hunter, L.K. Koopal, J. Lyklema, Measurement and interpretation of electrokinetic phenomena, Pure Appl. Chem. 77 (2005) 1753–1805.
[5] T.M.A. Papahadjopoulos, D.A. Gabizon, E. Mayhew, K. Matthay, S.K. Huang, K.D. Lee, M.C. Woodle, D.D. Lasic, C. Redemann, Sterically stabilized liposomes: improvements in pharmacokinetics and antitumor therapeutic efficacy, Proc. Natl. Acad. Sci. U. S. A. 88 (1991) 11460–11464.
[6] M.C. Woodle, Surface-modified liposomes: assessment and characterization for increased stability and prolonged blood circulation, Chem. Phys. Lipids 64 (1993) 249–262.
[7] M. Malmsten, S. Zauscher, Colloids and surfaces in biology, Curr. Opin. Colloid Interface Sci. 15 (2010) 393–394.

[8] J.F.L. Duval, K.J. Wilkinson, H.P. van Leeuwen, J. Buffle, Humic substances are soft and permeable: evidence from their electrophoretic mobilities, Environ. Sci. Technol. 39 (2005) 6435–6445.
[9] K.J. Wilkinson, J.R. Lead, Environmental colloids and particles: current knowledge and future developments, in: J.R.L. Kevin, J. Wilkinson (Eds.), Environmental Colloids and Particles: Behaviour, Separation and Characterisation IUPAC Series on Analytical and Physical Chemistry of Environmental Systems, John Wiley & Sons Ltd., Chichester, England; Hoboken, NJ, 2007.
[10] G. Francius, P. Polyakov, J. Merlin, Y. Abe, J. Ghigo, C. Merlin, C. Neloin, J.F.L. Duval, Bacterial surface appendages strongly impact nanomechanical and electrokinetic properties of *Escherichia coli* cells subjected to osmotic stress, Plos One 6 (2011) e20066.
[11] J.F.L. Duval, F. Gaboriaud, Progress in electrohydrodynamics of soft microbial particle interphases, Curr. Opin. Colloid Interface 15 (2010) 184–195.
[12] J. Rodríguez-López, H.C. Shum, L. Elvira, F. Montero de Espinosa, D.A. Weitz, Fabrication and manipulation of polymeric magnetic particles with magnetorheological fluid, J. Magn. Magn. Mater. 326 (2013) 220–224.
[13] S. Jiang, Z. Cao, Ultralow-fouling, functionalizable, and hydrolyzable zwitterionic materials and their derivatives for biological applications, Adv. Mater. 22 (2010) 920–932.
[14] A. Seminara, T.E. Angelinic, J.N. Wilking, H. Vlamakis, S. Ebrahime, R. Kolter, D.A. Weitz, M.P. Brenner, Osmotic spreading of *Bacillus subtilis* biofilms driven by an extracellular matrix, PNAS 109 (2012) 1116–1121.
[15] H. Ohshima, Electrophoresis of soft particles, Adv. Colloid Interf. Sci. 62 (1995) 189–235.
[16] H. Ohshima, Electrophoretic mobility of a charged spherical colloidal particle covered with an uncharged polymer layer, Electrophoresis 23 (2002) 1993–2000.
[17] H. Ohshima, Approximate expression for the electrophoretic mobility of a spherical colloidal particle covered with an ion-penetrable uncharged polymer layer, Colloid Polym. Sci. 283 (2005) 819–825.
[18] H. Ohshima, Electrophoresis of soft particles: analytic approximations, Electrophoresis 27 (2006) 526–533.
[19] H. Ohshima, Theory of Colloid and Interfacial Electric Phenomena, Elsevier, 2006.
[20] H. Ohshima, Electrokinetics of soft particles, Colloid Polym. Sci. 285 (2007) 1411–1421.
[21] H. Ohshima, Electrical phenomena of soft particles. A soft step function model, J. Phys. Chem. A 116 (2012) 6473–6480.
[22] G.J. Arrio, A. Carrette, J. Chevallier, D. Brethes, Electrokinetic and hydrodynamic properties of sarcoplasmic reticulum vesicles: a study by laser Doppler electrophoresis and quasi-elastic light scattering, Arch. Biochem. Biophys. 228 (1984) 20–229.
[23] D. Brethes, D. Dulon, G. Johannin, B. Arrio, T. Gulik-Krzywicki, J. Chevallier, Study of the electrokinetic properties of reconstituted sarcoplasmic reticulum vesicles, Arch. Biochem. Biophys. 246 (1986) 355–365.
[24] D. Brethes, D. Dulon, G. Johannin, B. Arrio, T. Gulik-Krzywicki, J. Chevallier, Study of the electrokinetic properties of reconstituted sarcoplasmic reticulum vesicles, Arch. Biochem. Biophys. 246 (1986) 355–365.
[25] P. Smejtek, L.E. Satterfield, R.C. Word, J.J. Abramson, Electrophoretic mobility of sarcoplasmic reticulum vesicles is determined by amino acids of A + P + N domains of Ca2 + −ATPase, Biochim. Biophys. Acta 1798 (2010) 1689–1697.
[26] R.J. Hill, D.A. Saville, W.B. Russel, Electrophoresis of spherical polymer-coated colloidal particles, J. Colloid Interface Sci. 258 (2003) 56–74.
[27] R.J. Hill, Hydrodynamics and electrokinetics of spherical liposomes with coatings of terminally anchored poly(ethylene glycol): numerically exact electrokinetics with self-consistent mean-field polymer, Phys. Rev. E. 70 (2004) 051406.
[28] J.A. Cohen, V.A. Khorosheva, Electrokinetic measurement of hydrodynamic properties of grafted polymer layers on liposome surfaces, Colloids Surf. A 195 (2001) 113–127.
[29] J.F.L. Duval, H. Ohshima, Electrophoresis of diffuse soft particles, Langmuir 22 (2006) 3533–3546.
[30] J. Langlet, F. Gaboriaud, C. Gantzer, J. Duval, Impact of chemical and structural anisotropy on the electrophoretic mobility of spherical soft multilayer particles: the case of bacteriophage MS2, Biophys. J. 94 (2008) 3293–3312.
[31] D.H. MacLennan, Purification and properties of an adenosine triphosphatase from sarcoplasmic reticulum, J. Biol. Chem. 245 (1970) 4508–4518.
[32] C. Toyoshima, Structural aspects of ion pumping by Ca^{2+}-ATPase of sarcoplasmic reticulum, Arch. Biochem. Biophys. 476 (2008) 3–11.
[33] C.A. Napolitano, P. Cooke, K. Segelman, L. Herbette, Organization of calcium pump protein dimers in the isolated sarcoplasmic reticulum membrane, Biophys. J. 42 (1983) 119–125.
[34] N. Reuter, K. Hinsen, J.-J. Lacapere, Transconformations of the SERCA1 Ca-ATPase: a normal mode study, Biophys. J. 85 (2003) 2186–2197.
[35] X. Shi, M. Chen, P.E. Huvos, P.M.D. Hardwicke, Amino acid sequence of a Ca^{2+} transporting ATPase from the sarcoplasmic reticulum of the cross-striated part of the abductor muscle of the deep sea scallop: comparison to serca enzymes of other animals, Comp. Biochem. Physiol. B 120 (1998) 359–374.
[36] K. Waku, Y. Uda, Y. Nakazawa, Lipid composition in rabbit sarcoplasmic reticulum and occurrence of alkyl ether phospholipids, J. Biochem. (Japan) 69 (1971) 483–491.